



# Optical Eratosthenes' sieve for large prime numbers

BOHAN LI,<sup>1</sup> GIORGIO MALTESE,<sup>2</sup> J. I. COSTA-FILHO,<sup>2</sup>  A. A. PUSHKINA,<sup>2</sup> AND A. I. LVOVSKY<sup>2,3,4,\*</sup>

<sup>1</sup>Department of Physics, Hong Kong University of Science and Technology, Clear Water Bay, Kowloon, Hong Kong, China

<sup>2</sup>Department of Physics, University of Oxford, Oxford, OX1 3PU, UK

<sup>3</sup>Russian Quantum Center, 100 Novaya St., Skolkovo, Moscow, 143025, Russia

<sup>4</sup>P. N. Lebedev Physics Institute, Leninskiy prospect 53, Moscow, 119991, Russia

\*alex.lvovsky@physics.ox.ac.uk

**Abstract:** We report the first experimental demonstration of a prime number sieve via linear optics. The prime numbers distribution is encoded in the intensity zeros of the far field produced by a spatial light modulator hologram, which comprises a set of diffraction gratings whose periods correspond to all prime numbers below 149. To overcome the limited far field illumination window and the discretization error introduced by the spatial light modulator finite spatial resolution, we rely on additional diffraction gratings and sequential recordings of the far field. This strategy allows us to optically sieve all prime numbers below  $149^2 = 22201$ .

© 2020 Optical Society of America under the terms of the [OSA Open Access Publishing Agreement](#)

## 1. Introduction

The study of prime numbers, although millenia old, is still a trending topic in mathematics. On the theoretical side, there are relevant fundamental problems which remain open, such as the Riemann hypothesis and the primes' distribution [1,2]. On a more applied note, prime factorization, which is the cornerstone of modern cryptography [3,4], motivates a search for more efficient algorithms.

In the past decades, physics emerged as a fruitful venue for progress on prime numbers research. Most efforts were focused on factorization, culminating in the celebrated Shor's algorithm [5] and the current quest for practical quantum computers. However, the application of analogue physical tools for more fundamental mathematical problems is also being investigated, for example with respect to the Riemann hypothesis [6–9].

A new and relatively unexplored testbed for the connection between physics and prime numbers is classical optics. On the factorization front, interferometric [10,11] and optoelectronically assisted algorithms [12] schemes have been proposed, and experimental demonstrations were carried out based on the Talbot effect [13,14] and polychromatic interference in a multipath interferometer [15]. On the fundamental side, Berry [16,17] proposed the reading of Riemann function's zeros from radiation patterns using the property of the far field propagation to represent the Fourier transform.

Inspired by Berry's proposal, Petersen et al. [18] have recently proposed a physical prime numbers sieve based on the superposition of identical waves. The scheme is based on the sieve of Eratosthenes [19], one of the oldest algorithms for finding prime numbers. Given the sequence of integers  $n$  from 2 to  $M$ , Eratosthenes' sieve iteratively discards their multiples, such that all remaining integers lower than  $M^2$  are necessarily primes. Reference [18] proposes to realize the sieving by gratings of equally spaced  $n$  point-like sources: in the far field profile, each grating interferes constructively at locations corresponding to the multiples of  $n$ , and destructively at other integers. The pattern resulting from all these gratings has the prime numbers encoded in its intensity zeros, and locating them permits the realization of the sieve.

In this paper, we implement and further develop the scheme devised in [18] by means of a phase-only spatial light modulator (SLM), where the apertures are realized by phase masks illuminated by a monochromatic laser. The far field intensity profile is measured by a CMOS camera, and the optical sieve corresponds to intensity minima of that profile. By making use of additional diffraction gratings and sequential camera acquisitions we can extend the sieving range beyond the pixel resolution of the SLM and the camera. The only remaining limitation associated with the SLM pixel resolution is the number of gratings that can be fitted in the phase mask. Capped by this limitation, we demonstrate an optical sieve capable of identifying all prime numbers below  $149^2 = 22201$ .

## 2. Theory

### 2.1. Sieving mask

To illustrate the optical sieve proposed in [18], consider an amplitude grating of  $n$  equally spaced point-like sources, aligned along the horizontal direction  $x$  and with spatial frequency  $1/n$ :

$$g_n(x) = \sum_{i=0}^{n-1} \delta(x - i/n), \quad (1)$$

where  $\delta(x)$  is the Dirac delta function. This can equivalently be seen as an infinite grating of pinholes illuminated by a plane monochromatic wave over a unit length window, as shown in Fig. 1. Since far field propagation corresponds to taking a Fourier transform

$$\tilde{g}_n(q_x) = \int_{-\infty}^{\infty} g_n(x) e^{-2\pi i x q_x} dx, \quad (2)$$

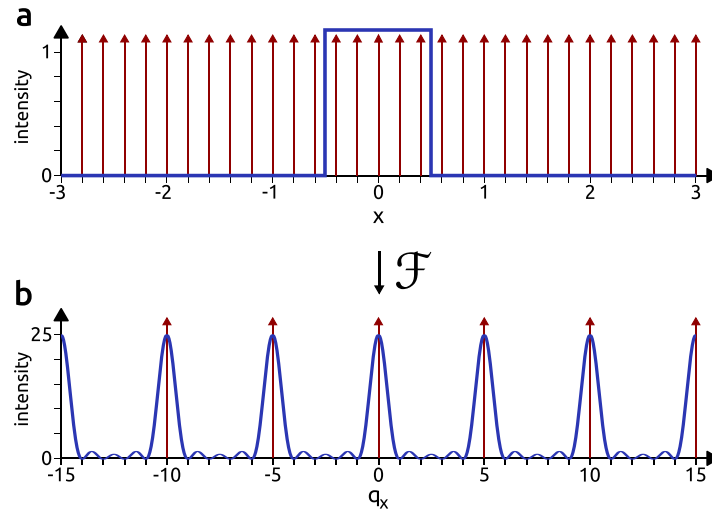


**Fig. 1.** Light intensity profiles at near (a) and far (b) fields, for  $n = 5$  pinholes per unit length. Red arrows represent an infinite array of pinholes and the corresponding effect on the far field. When this array is restricted to five pinholes [which corresponds to multiplication by the blue envelope in (a)], the far field pattern (which is the result of a Fourier transformation  $\mathcal{F}$  of the near field) becomes convolved with a sinc function, but the intensity at all integers except multiples of 5 remains at zero.

where  $q_x$  is the horizontal coordinate in the far field plane, this configuration generates a field

$$\tilde{g}_n(q_x) = \left( n \sum_{j=-\infty}^{\infty} \delta(q_x - nj) \right) * \text{sinc}(q_x), \quad (3)$$

where  $\text{sinc}(t) = \sin(\pi t)/\pi t$ , of equally spaced peaks (due to the pinholes) convolved with a sinc envelope (due to the illumination window). The resulting intensity pattern has zeros at all integers except the multiples of  $n$ .

Superposing, in the object plane, these gratings  $g_n$  for  $n \in \{2, 3, 5, \dots, M\}$  leads to a far field interference pattern where, akin to the sieve of Eratosthenes, the multiples of the  $n$ 's are "discarded" (by becoming intensity peaks) and the remaining zeros correspond to  $q_x$  being a prime number. Therefore, via the mapping of the far field zeros, the scheme sieves the prime numbers in the range  $M' \leq q_x < M'^2$ , where  $M'$  is the next prime after  $M$ .

The superposition of gratings (which we refer to as the *sieving mask*) can be implemented by displaying each of them at a different vertical position, as shown in Fig. 2 (left column). In the far field plane, Fig. 2 (centre column), the waves from different gratings interfere, but the intensity at the primes'  $q_x$  positions remains zero for all  $q_y$ . Therefore, a horizontal profile of the far field [Fig. 2 (right column)], obtained by integration along  $q_y$ , allows sieving of the prime numbers as described before.

## 2.2. Displacement grating

The above treatment assumes ideal point-like pinholes. A more realistic model would consider finite-size rectangular apertures, as depicted in Fig. 2(b), which are mathematically represented by the convolution

$$E_n(x) = g_n(x) * T_w(x), \quad (4)$$

where  $T_w(x)$  is the top-hat function and  $w$  is the aperture width. The resulting far field pattern will be modulated by a sinc envelope  $\text{sinc}(wq_x)$ . This envelope affects the pattern's visibility, which progressively degrades for higher values of  $|q_x|$ , and also introduces additional zeros, which do not correspond to prime numbers. In practice, it limits the sieve's working range to the central lobe of the sinc.

This issue is addressed by adding a position-dependent linear function, dubbed here *displacement grating*, to the phase to each aperture [Fig. 2(c)]:

$$g'_n(x) = g_n(x) e^{i2\pi x d_x}. \quad (5)$$

It results in a spatial shift of the intensity zeros by  $d_x$  in the  $q_x$  coordinate of the far field,

$$\tilde{g}'_n(q_x) = \tilde{g}_n(q_x - d_x) \quad (6)$$

so that

$$\tilde{E}'_n(x) = \tilde{g}'_n(q_x) \cdot w \text{sinc}(wq_x). \quad (7)$$

Because we keep the phase inside each aperture constant, the modulation envelope  $\text{sinc}(wq_x)$  remains undisplaced. By progressively increasing the slope  $d_x$  of the displacement grating we are able to scan different sections of the Eratosthenes' sieve over the central lobe of the sinc envelope, therefore covering the full sieving range.

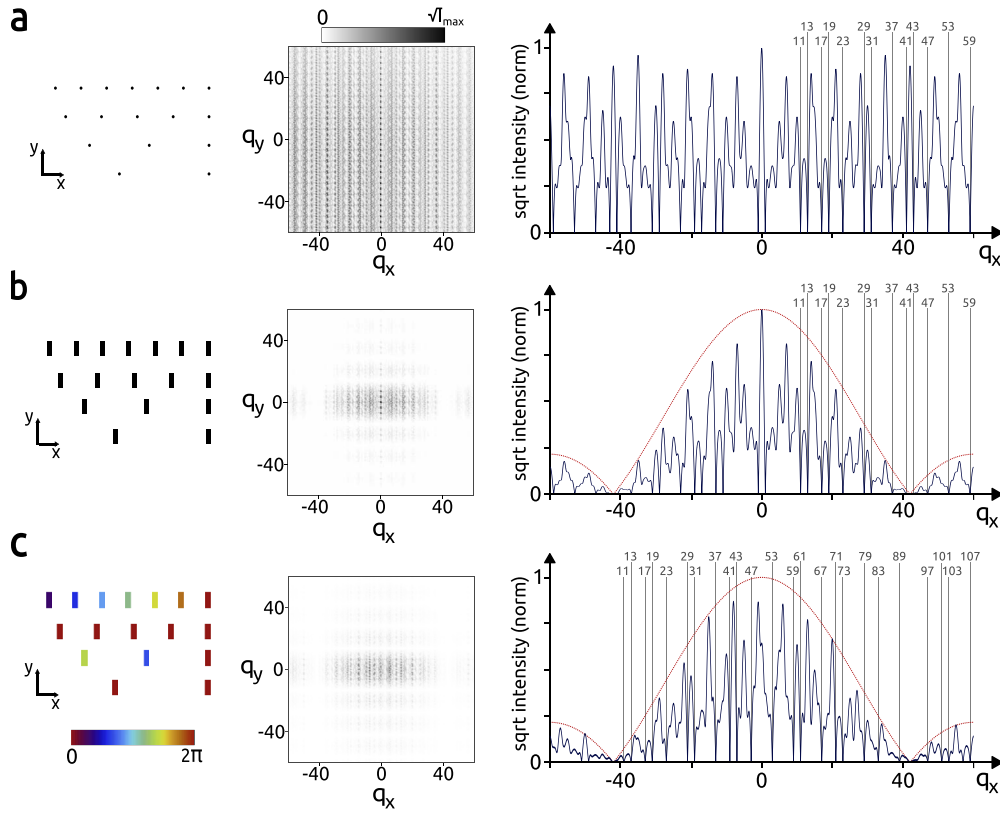


**Fig. 2.** Optical sieve diffraction mask (left) in the case of  $\{n\} = \{2, 3, 5, 7\}$ . The square root of the corresponding far field intensity profile (centre) and its horizontal marginal (integral over  $q_y$ , right), which reveals the prime numbers in the intensity zeros, highlighted by vertical grey lines. (a) Sieving mask proposed in [18], composed of point-like apertures. (b) Sieving mask with finite-size rectangular apertures of width  $w = 1/42$ . (c) Sieving mask superposed with displacement grating, which shifts the primes distribution by  $d_x = 50$ .

### 3. Experiment

As illustrated in the scheme of the experimental setup in Fig. 3(a), the optical prime sieve consists of a phase-only liquid crystal on silicon (LCoS) SLM illuminated almost uniformly by a continuous-wave laser (Eagleyard EYP-DFB-0785 with  $\lambda = 785$  nm) beam, along with a camera placed in its far field.

The spatial profile of the emitted laser beam is filtered by a single mode fibre and magnified by a telescope before illuminating the SLM screen. At the SLM, the laser power is approximately 0.1mW. The phase-only LCoS-SLM (Hamamatsu X13138-02) has a spatial resolution of  $1280 \times 1024$  pixels, 12.5 $\mu$ m pixel pitch, 60Hz refresh rate and 256 input signal levels.

A set of optical lenses ( $f_1 = 250$ mm,  $f_2 = 75$ mm,  $f_3 = 150$ mm) produces and magnifies the far field pattern. A monochrome CMOS sensor (uEye UI-3270 CP-M-NO-R2), of pixel pitch 3.45 $\mu$ m, aligned with the SLM diagonal and anti-diagonal axis, acquires the far field intensity profile. The camera spatial resolution ( $2056 \times 1542$  pixels) and the chosen optics allow a proper spatial sampling rate, with approximately 10 camera pixels corresponding to  $\Delta q_x = 1$ . The camera's digitiser is set to 12-bit depth and the exposure time to 3.15 ms, to maximize intensity resolution and avoid saturation.

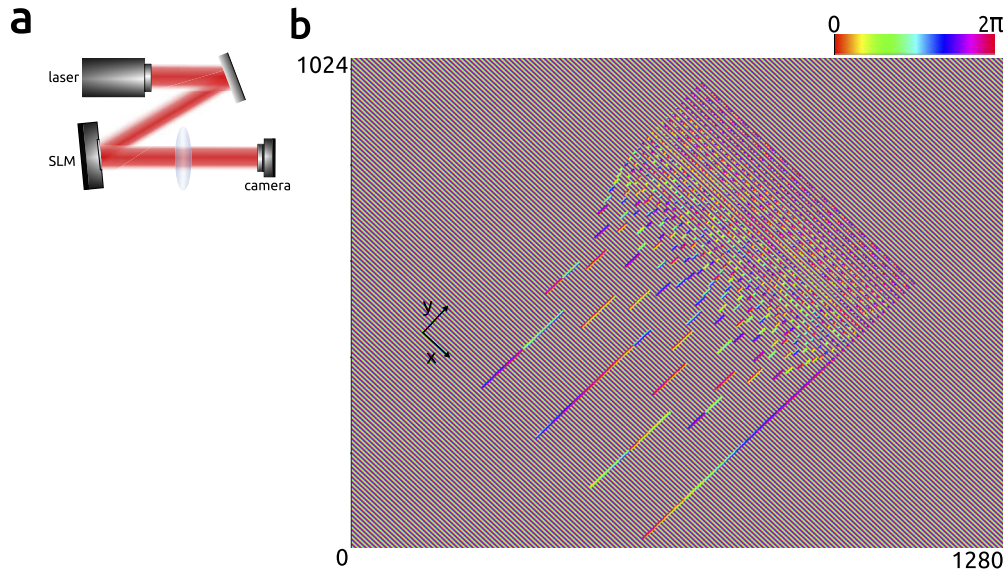


**Fig. 3.** Experimental implementation of the optical prime sieve. a) Scheme of the experiment. b) Phase mask hologram as displayed on the SLM screen.

The sieving mask is implemented by phase holograms in the SLM screen, as exemplified in Fig. 3(b). The background outside the “apertures” is filled with a blazed grating whose lines are oriented along the  $x$  axis. The function of this grating is to diffract the light away from the sieving area, so only the light reflected from the apertures is captured by the camera. The mask is arranged diagonally at  $45^\circ$ , in order to prevent the light scattered from both the SLM screen borders and the space between pixels, in the horizontal and vertical directions, from contaminating the image (in the laboratory reference frame, the SLM is mounted upright and the camera is physically tilted). Additionally, we apply a linear phase displacement to the apertures, i.e. we multiply  $E'_n(x)$  by  $e^{i2\pi xd_0}$ , which displaces the entire far field pattern by  $d_0$ , thereby separating it from the SLM screen’s specular reflection.

The patterns printed on the SLM extend over 420 pixels along  $x$ , accommodating apertures which are 3 pixels wide, corresponding to the effective width  $w = 1/140$ . These patterns include gratings corresponding to prime numbers up to  $M = 139$ , allowing a sieving range of  $139 < q_x < 149^2 = 22201$ , 149 being the next prime number after 139. The displacement gratings’ slopes  $d_x$  are varied from zero to 22180 in increments of  $R = 40$ , covering the whole sieving range. While the size of the central lobe of the sinc function is  $2/w = 280$ , we chose a smaller increment value for higher contrast.

To improve the contrast, we set the slits’ length along  $y$  to  $\text{round}(200/n)$  pixels, so that each grating  $g_n$  contributes equally to the far field intensity pattern. We substitute  $g_2$  and  $g_3$  by pairs of gratings with  $n = 4$  and  $n = 6$ , respectively, in order to reduce the space required by the grating with the longest slits. Additional displacement gratings are applied to one element of each pair so the collective action of the pair of elements is equivalent to that of  $g_2$  and  $g_3$ . Further, we extend the total length of  $g_4$  by a factor of 1.6, since it is located close to the SLM screen border and the laser power distribution, which is not perfectly uniform, is slightly lower there.

A key requirement on the optical prime sieve is the even spacing of its apertures, combined with their precise positioning. This is difficult to achieve in practice given a large number of gratings that need to be printed, as well as the finite SLM pixel resolution. If the apertures’

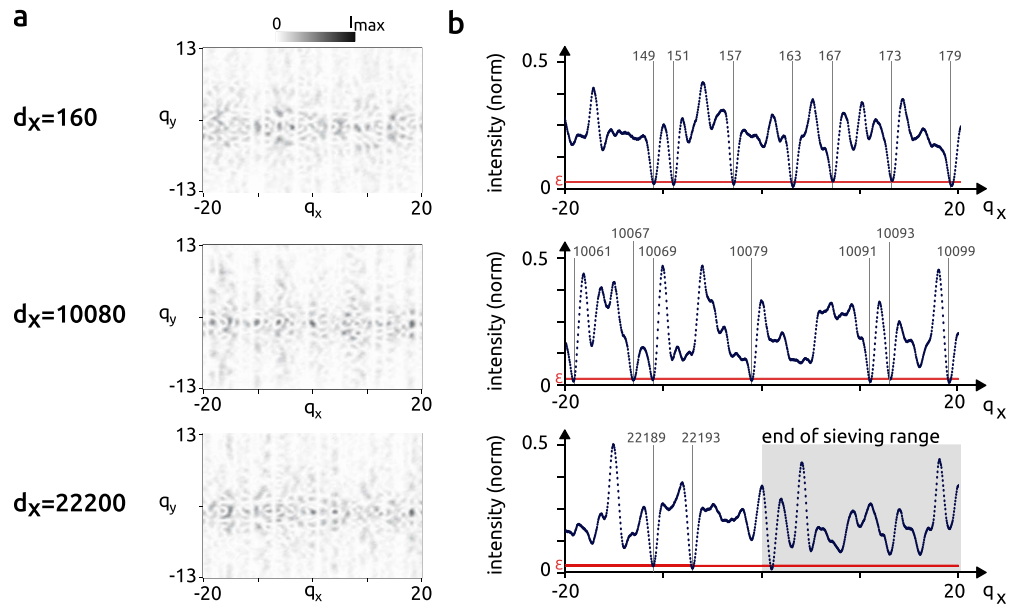


spacing is rounded to the closest integer, the far field pattern becomes severely distorted and can no longer be used for sieving [Fig. 5(a,b)].

This distortion is significant when the function  $\tilde{g}_n(\cdot)$  has a large argument, i.e., according to Eq. (6), for large displacement grating slopes  $d_x$ . We address this issue by recalling that each function  $\tilde{g}_n(\cdot)$  is periodic with zeros at the integers not multiples of  $n$ . Hence displacing it by  $d_x$  is equivalent to displacing it by the remainder of the division of  $d_x$  by  $n$ . Therefore the slope of each displacement grating can be modified according to  $d_x^{(n)} = d_x \bmod n$  without any effect on the sieve, albeit at the cost of a different displacement slope for each line  $g_n$ . The effect of this correction is illustrated in Fig. 5(c). This compensation allows us to keep the argument of  $\tilde{g}_n(\cdot)$  low for all  $g_n$ , thereby achieving correct sieving.

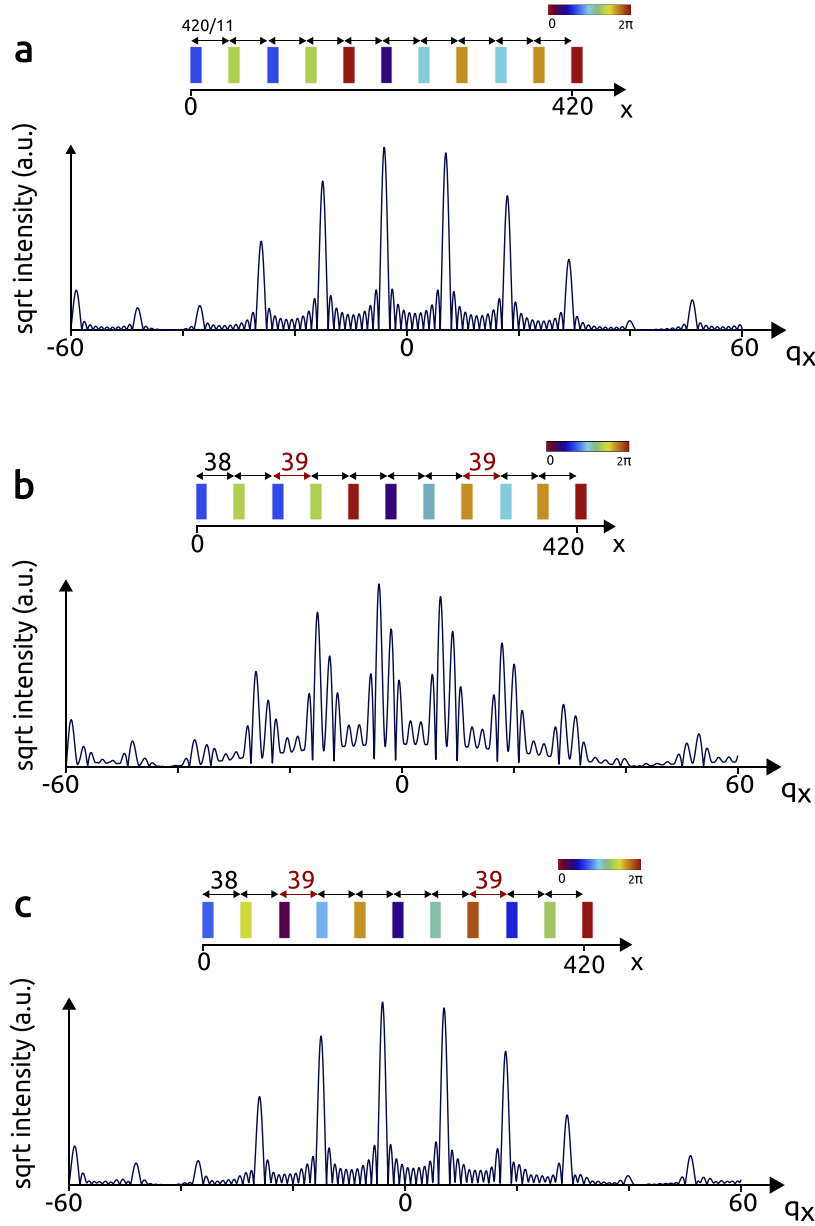
The aberrations of the setup, due to both the lenses along the optical path and the intrinsic SLM curvature, distort the wavefront of the diffracted beam, reducing its spatial coherence and thus the interference visibility. This is corrected by adding a global phase profile to the SLM mask, which is measured via the calibration method proposed in [20].

Figure 4(a) shows the recorded far field intensity image for the SLM holograms of Fig. 3(b). To maximize the contrast between primes zeros and composites minima, each recorded frame is integrated over 600 pixels along  $q_y$ , generating an average intensity plot  $I(q_x)$  [Fig. 4(b)]. During this operation, we also subtract the background noise, recorded after applying to the SLM a hologram without the apertures. To cover the whole sieving range, we need to acquire  $22000/40 = 550$  frames. When the intensity value  $I(q_x)$  is lower than the threshold  $\epsilon$ ,  $q_x$  is labeled as a prime.



**Fig. 4.** Experimental results. a) Far field intensity images as acquired by the camera for different displacement grating slopes  $d_x$ , rescaled into the units of  $q_x, q_y$ . b) Integrals of the acquired intensity images along  $q_y$ . All minima below the intensity threshold  $\epsilon$  (horizontal red line) are classified as prime numbers (vertical grey lines).

We find that an intensity threshold that is in between 4.8% and 5.9% of the global maximum allows us to correctly sieve all the primes (2436 numbers) and discard all the composites (19626 numbers) within the sieving range (Fig. 6). This range quantifies the robustness of our scheme.



**Fig. 5.** Effect of the SLM's spatial resolution on the produced far field intensity profile for  $n = 11$  and a displacement grating of slope  $d_x = 180$  (theoretical model). (a) Evenly spaced apertures (infinite resolution); (b) Discrete pixels with a total pattern width of  $W = 420$  pixels: the apertures are spaced by either 38 or 39 pixels. The integers not multiples of 11 are no longer zeros in the far field intensity profile. (c)  $W = 420$  with a displacement grating of slope  $d_x^{(11)} = 180 \bmod 11 = 4$ : the desired structure of the far field is closely restored.

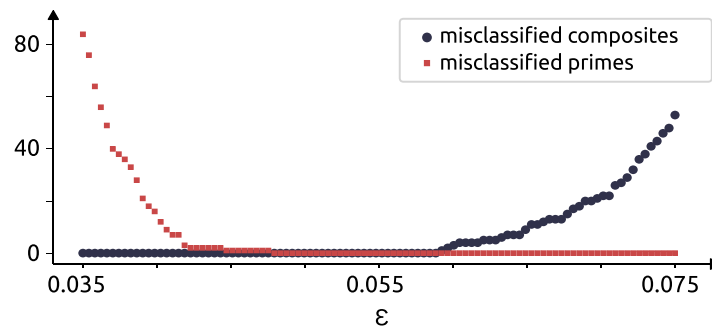


**Fig. 6.** Number of misclassified primes (red squares) and composites (blue dots) within the measured sieving range  $139 < q_x < 22201$  as a function of the intensity threshold  $\epsilon$ . By choosing  $0.048 < \epsilon < 0.059$ , the optical sieve correctly sieves all primes and discards composites.

#### 4. Discussion

This work is the first experimental realization of an optical prime number sieve. By generating high resolution and on-demand phase masks via an SLM, we prove the effectiveness of the sieve by correctly classifying integers up to 22201 as either primes or composites.

The scalability of the sieving range, dictated by the number of apertures that can be fitted in a phase mask, is ultimately limited by the SLM spatial resolution. It is also limited by the SLM refresh rate, since a sequence of images has to be displayed in order to cover the whole sieving range. As SLM technology improves with respect to these two features, we expect better optical sieves to be implemented. The principally achievable range of the sieve can be estimated as the square of the SLM pixel resolution.

Note, however, that calculating the corrected displacement grating for each displacement  $d_x$  involves multiple modulo operations, which is equivalent, in terms of computational complexity, to checking the primality of  $d_x$ . Therefore our technique does not completely eliminate this type of calculations, but only reduces it by a factor equal to the increment value  $R$ . This value is limited by the width  $2/w$  of the central lobe of the function  $\text{sinc}(wq_x)$ , and hence cannot exceed the doubled SLM resolution.

Our method can be straightforwardly adapted to other kinds of sieves, such as Gaussian or twin primes sieves [18]. More generally, it demonstrates the potential of free-space linear optics in tasks that transcend imaging or communication, such as computation and solving mathematical problems. We can leverage the spatial coherence and superposition properties of light to achieve parallelism in computing.

#### Funding

Russian Science Foundation (19-71-10092).

#### Disclosures

The authors declare that there are no conflicts of interest related to this article.

#### References

1. A. E. Ingham, *The distribution of prime numbers* (Cambridge University, 1990).
2. H. M. Edwards, *Riemann's Zeta Function* (Dover Publications, 2001).
3. R. L. Rivest, A. Shamir, and L. Adleman, "A method for obtaining digital signatures and public-key cryptosystems," *Commun. ACM* **21**(2), 120–126 (1978).



4. A. J. Menezes, P. C. van Oorschot, and S. A. Vanstone, *Handbook of Applied Cryptography (Discrete Mathematics and Its Applications)* (CRC Press, 1996).
5. P. Shor, "Polynomial-time algorithms for prime factorization and discrete logarithms on a quantum computer," *SIAM J. Comput.* **26**(5), 1484–1509 (1997).
6. D. Schumayer and D. A. W. Hutchinson, "Colloquium: Physics of the Riemann hypothesis," *Rev. Mod. Phys.* **83**(2), 307–330 (2011).
7. C. M. Bender, D. C. Brody, and M. P. Müller, "Hamiltonian for the zeros of the Riemann zeta function," *Phys. Rev. Lett.* **118**(13), 130201 (2017).
8. L. A. Bunimovich and C. P. Dettmann, "Open circular billiards and the Riemann hypothesis," *Phys. Rev. Lett.* **94**(10), 100201 (2005).
9. M. V. Berry and J. P. Keating, "The Riemann zeros and eigenvalue asymptotics," *SIAM Rev.* **41**(2), 236–266 (1999).
10. A. A. Rangelov, "Factorizing numbers with classical interference: several implementations in optics," *J. Phys. B: At., Mol. Opt. Phys.* **42**(2), 021002 (2009).
11. J. F. Clauser and J. P. Dowling, "Factoring integers with Young's n-slit interferometer," *Phys. Rev. A* **53**(6), 4587–4590 (1996).
12. A. Shamir, "Factoring large numbers with the TWINKLE device," *International Workshop on Cryptographic Hardware and Embedded Systems* (Springer, 1999), pp. 2–12.
13. D. Bigourd, B. Chatel, W. P. Schleich, and B. Girard, "Factorization of numbers with the temporal Talbot effect: Optical implementation by a sequence of shaped ultrashort pulses," *Phys. Rev. Lett.* **100**(3), 030202 (2008).
14. K. Pelka, J. Graf, T. Mehringer, and J. von Zanthier, "Prime number decomposition using the Talbot effect," *Opt. Express* **26**(12), 15009–15014 (2018).
15. V. Tamma, H. Zhang, X. He, A. Garuccio, W. P. Schleich, and Y. Shih, "Factoring numbers with a single interferogram," *Phys. Rev. A* **83**(2), 020304 (2011).
16. M. V. Berry, "Riemann zeros in radiation patterns," *J. Phys. A: Math. Theor.* **45**(30), 302001 (2012).
17. M. V. Berry, "Riemann zeros in radiation patterns: II. Fourier transforms of zeta," *J. Phys. A: Math. Theor.* **48**(38), 385203 (2015).
18. T. C. Petersen, M. Ceko, I. D. Svalbe, M. J. Morgan, A. I. Bishop, and D. M. Paganin, "Simple wave-optical superpositions as prime number sieves," *Phys. Rev. Lett.* **122**(9), 090201 (2019).
19. R. Crandall and C. B. Pomerance, *Prime numbers: a computational perspective* (Springer Science & Business Media, 2006), 2nd ed.
20. T. Čížmár, M. Mazilu, and K. Dholakia, "In situ wavefront correction and its application to micromanipulation," *Nat. Photonics* **4**(6), 388–394 (2010).